CELLULAR NEUROSCIENCE

Widespread posttranscriptional regulation of cotransmission

Nannan Chen[1]†, Yunpeng Zhang[1]†, Emmanuel J. Rivera-Rodriguez[1]†, Albert D. Yu[1,2], Michael Hobin[1], Michael Rosbash[1,2], Leslie C. Griffith[1]*

While neurotransmitter identity was once considered singular and immutable for mature neurons, it is now appreciated that one neuron can release multiple neuroactive substances (cotransmission) whose identities can even change over time. To explore the mechanisms that tune the suite of transmitters a neuron releases, we developed transcriptional and translational reporters for cholinergic, glutamatergic, and GABAergic signaling in *Drosophila*. We show that many glutamatergic and GABAergic cells also transcribe cholinergic genes, but fail to accumulate cholinergic effector proteins. Suppression of cholinergic signaling involves posttranscriptional regulation of cholinergic transcripts by the microRNA miR-190; chronic loss of miR-190 function allows expression of cholinergic machinery, reducing and fragmenting sleep. Using a "translation-trap" strategy, we show that neurons in these populations have episodes of transient translation of cholinergic proteins, demonstrating that suppression of cotransmission is actively modulated. Posttranscriptional restriction of fast transmitter cotransmission provides a mechanism allowing reversible tuning of neuronal output.

INTRODUCTION

Small-molecule chemicals mediating neuronal communication are packaged into vesicles for release by vesicular neurotransmitter transporter proteins (vNTs). The most common fast-acting neurotransmitters in both vertebrates and invertebrates each have a cognate vNT (or vNT family): VAChT for acetylcholine (ACh), VGAT for γ-aminobutyric acid (GABA), and VGluT for glutamate (Glu) (*1*). Cotransmission, release of multiple neuroactive molecules from a single cell, has been reported in many animals and usually involves release of a bioamine or peptide neuromodulator with a fast transmitter (*2*, *3*). This type of modulation can be regulated by changes in environment or neuronal activity (*4*). Cotransmission between multiple fast-acting neurotransmitters has only been seen functionally in a few cases (*5*, *6*), although some studies have reported the coexpression of multiple vNT mRNAs (*7*–*9*). Such cotransmission can have profound effects on circuit dynamics (*10*, *11*). Using newly developed genetic tools to study transcription and translation of vNTs for fast neurotransmitters, we demonstrate here that there are large populations of fully differentiated glutamatergic and GABAergic neurons in the adult fly brain that transcribe genes specifying synthesis and release of ACh but block accumulation of protein products via microRNA (miR) repression. This suggests a widespread, but tightly regulated, potential for cotransmission.

RESULTS

To map the extent of cotranscription of vNTs, we used a split-GAL4 strategy (*12*) in which GAL4-DNA binding domain (DBD) or activation domain (AD) sequences were inserted into the endogenous loci of the *VAChT*, *VGluT*, and *VGAT* genes to put them under the control of NT-specific transcriptional programs (Fig. 1A and fig. S1A). Both the *VGluT-AD:VAChT-DBD* (Fig. 1B) and *VAChT-AD:VGluT-DBD* (fig. S1C) split-GAL4s show broad expression with the strongest signal in fan-shaped body (FSB) neurons. As expected for intersectional drivers, *VAChT:VGluT* split-GAL4 labels fewer neurons than either *VAChT*- or *VGluT-GAL4* drivers (fig. S1B). We will refer to the cell subset labeled by this intersectional tool as "Glu^{ACh}" neurons and the split-GAL4 as *Glu^{ACh}-GAL4*. Similarly, both the *VGAT-AD:VAChT-DBD* (Fig. 1C) and *VAChT-AD:VGAT-DBD* (fig. S1D) split-GAL4s had a broad but distinct expression profile, with the strongest enhanced green fluorescent protein (EGFP) signal in ellipsoid body (EB) neurons; we call these cells "GABA^{ACh}" neurons. *VGAT:VGluT* split-GAL4 brains showed no consistent coexpression, only a few EB cells from multiple ring neuron subtypes (fig. S1, E and F). These results suggested potential coexpression of *VAChT* with both the *VGluT* and *VGAT* genes and possible cotransmission in a substantial number of cells.

To verify cotranscription of the native vNT genes in these cells, we analyzed polyadenylated nuclear RNA (polyA-RNA)from "isolation of nuclei tagged in specific cell types" (INTACT)–sorted Glu^{ACh} and GABA^{ACh} nuclei (Fig. 1D) (*13*). We chose to measure nuclear mRNA as it is a better reporter of transcription than bulk RNA sequencing (RNA-seq) because posttranscriptional cytoplasmic processes that can degrade mRNAs do not have access to this pool of message. Because these posttranscriptional processes are critical for setting steady-state mRNA levels in the cytoplasm, the relative levels of transcript reported by nuclear RNA-seq may be different than typically seen with bulk RNA-seq methods that were mRNA regulated by degradation, e.g., by RNA-induced silencing complex or in P-bodies, which would be depleted (*14*). As expected, GABA^{ACh} nuclei express high levels of *GAD1* and *GAT* mRNA, while Glu^{ACh} nuclei express high levels of *VGluT. VAChT*, *ChaT*, and *ChT* mRNAs are also expressed strongly in the nuclear mRNA of both cell types. *Portabella* and *CG13646*, vNTs related to VAChT/VGluT and VGAT, respectively, were not found at significant levels in either population.

[1]Department of Biology, Volen National Center for Complex Systems, Brandeis University, Waltham, MA 02454-9110, USA. [2]Howard Hughes Medical Institute, Brandeis University, Waltham, MA 02454-9110, USA.
*Corresponding author. Email: griffith@brandeis.edu
†These authors contributed equally to this work.

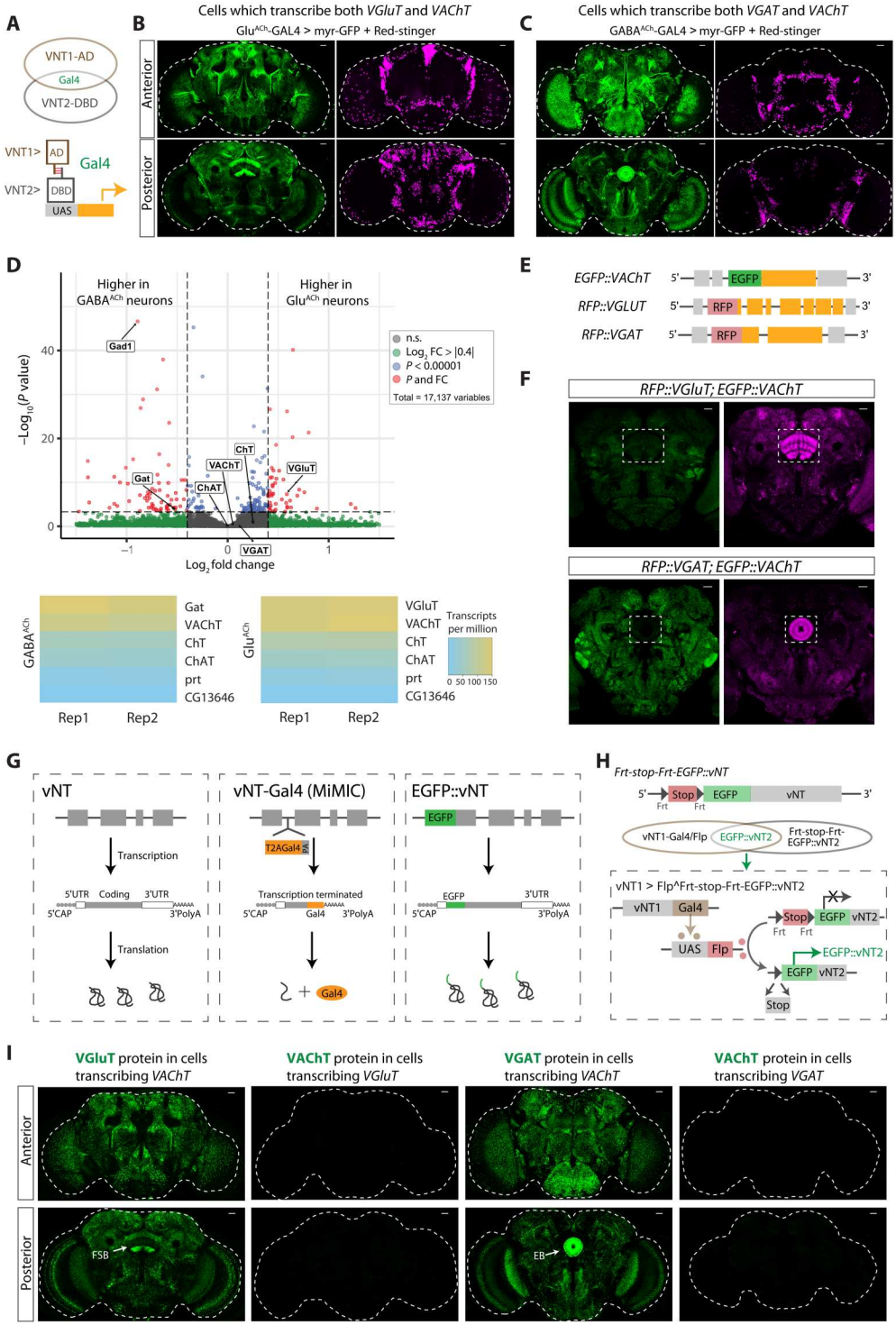

Fig. 1. *VAChT* is transcribed in VGluT- and VGAT-positive neurons. (**A**) Split-GAL4 strategy. Coexpression of AD and DBD reconstitutes GAL4 to initiate transcription. (**B** and **C**) Expression patterns of *VGluT-AD;VAChT-DBD split-GAL4* (B) and *VGAT-AD;VAChT-DBD split-GAL4* (C) anterior (top) and posterior (bottom). Green marks neuronal membrane, and magenta marks nuclei. Dashed lines outline the brain. (**D**) Nuclear RNA-seq demonstrates high cholinergic mRNA levels in Glu^{ACh} and $GABA^{ACh}$ neurons. Volcano plot (top) shows statistically significant enrichment of *VGluT* in Glu^{ACh} cells [adjusted *P* value (P_{adj}) < 0.05; log_2 fold change (log_2FC) = 0.58] as well as Gat (P_{adj} < 0.05; log_2FC = −0.52) and Gad1 (P_{adj} < 0.05; log_2FC = −0.89) in $GABA^{ACh}$ neurons. *VAChT*, *ChaT*, and *ChT* were not differentially expressed (P_{adj} > 0.05). Heatmaps (bottom) show cholinergic markers present in both cell types at levels comparable to *VGluT* and *VGAT*. Control vesicular transporters are not expressed. (**E**) N-terminal genomic fusion lines. (**F**) Representative single-slice pictures of adult brains of *RFP::VGluT;EGFP::VAChT* (top) and *RFP::VGAT; EGFP::VAChT* (bottom) flies. Green indicates EGFP while magenta indicates RFP. Dashed boxes indicate positions of FSB (top) and EB (bottom). (**G**) Schematic showing transcription and processing of vNT mRNA in wild-type (left), MiMIC-derived T2A GAL4 alleles (middle), and EGFP::vNT fusion alleles (right). For vNT-GAL4 alleles, transcription is terminated after GAL4, inducing loss of vNT 3′ untranslated region (3′UTR) information. For EGFP::vNT alleles, EGFP is transcribed and translated as part of the intact vNT mRNA. (**H**) Flip-out-stop strategy. vNT1-$GAL4^{MIMiC}$ drives FLP recombinase, excising the FRT-flanked stop cassette preceding EGFP::vNT2. EGFP signal therefore indicates transcription of vNT1 with transcription and translation of vNT2 in the same neuron. (**I**) *VAChT-GAL4* flip-out derepression of EGFP::VGluT shows EGFP in FSB, while *VAChT-GAL4* flip out of EGFP::VGAT shows EGFP in EB. Flip-out derepression ECFP::VAChT shows no signal. Dashed lines outline brain. Scale bars, 20 μm. n.s., not significant.

To be functionally cotransmitting, Glu^{ACh} and $GABA^{ACh}$ neurons would need to express the protein products of both vNT genes. To directly visualize the vNT proteins, we fused fluorescent proteins (FPs) to the N termini of the endogenous coding sequences using CRISPR-Cas9 (Fig. 1E). These fusion alleles faithfully recapitulate the native protein distribution as assessed by immunostaining of heterozygotes (fig. S2), indicating that the gene manipulations did not change expression patterns. Costaining for EGFP and red fluorescent protein (RFP) in *RFP::VGluT;EGFP::VAChT* fly brains, we found strong RFP::VGluT protein expression in FSB neurons, but no EGFP::VAChT protein at the same level of the confocal stack (Fig. 1F). Similarly, in *RFP::VGAT;EGFP::VAChT* fly brains, strong RFP::VGAT staining is present in EB neurons, but EGFP::VAChT protein is not (Fig. 1F).

While split-GAL4 expressed from the *VAChT* locus is present in FSB and EB, the lack of EGFP::VAChT protein indicates that the gene product does not accumulate in these regions. We hypothesized that the difference might be a function of the structure of the *VAChT* transcripts produced in these two different CRISPR-engineered animals. For *VAChT* split-GAL4 lines [and the T2A-GAL4 *Minos*-mediated integration cassette (MiMIC) lines used below], GAL4 coding sequence(s), followed by a polyadenylation site, are inserted into a vNT intron, producing a truncated transcript that lacks the vNT gene's 3′ untranslated region (3′UTR), a region that can contain cis-regulatory sequences regulating translation and/or RNA stability (*15*). For FP::vNT fusion alleles, the FP coding sequence is fused in frame to form a functional chimeric vNT protein, meaning that the FP::vNT mRNA has all the regulatory information native to the wild-type vNT mRNA (Fig. 1G). This suggests that, while both the *VAChT* split-GAL4 and *EGFP::VAChT* mRNA are transcribed in Glu^{ACh} and GABA^{ACh} neurons, mRNA containing native 3′UTR sequences is not translated. The presence or absence of the native 3′UTR for all the lines used in this study is shown in table S1.

To test the idea that the 3′UTR was important for protein expression, we created conditional FP fusion alleles containing an *Frt-stop-Frt-FP* cassette downstream of the start codon of each vNT gene (Fig. 1H). In these animals, FP::vNT transcription is blocked until FLP recombinase is expressed, excising the stop cassette. GAL4^{+} cells then become competent to generate an FP::vNT mRNA containing all the endogenous gene's UTR information. *Frt-stop-Frt-ECFP::VAChT* flies were validated by driving FLP expression with *VT030559-GAL4* in cholinergic mushroom body cells. ECFP::VAChT was present in mushroom body as expected and dependent on GAL4 (fig. S3A). Similarly, EGFP::VGluT in FSB neurons and EGFP::VGAT signal in the anterior paired lateral neurons demonstrate the specificity of these lines (fig. S3, B and C).

Figure 1H shows the strategy used to test for posttranscriptional suppression of VAChT protein expression in Glu^{ACh} and GABA^{ACh} neurons. Expression of "vNT1-GAL4," which captures transcription of vNT1 but lacks a native 3′UTR that might suppress GAL4 protein expression, drives FLP recombinase to catalyze excision of the stop cassette for "FP::vNT2." Only if the cells that transcribe vNT1 are also competent to both transcribe and translate vNT2, then an FP signal is seen. Using *VAChT-GAL4* to flip out the stop cassette for *EGFP::VGluT* results in strong protein signal in the same pattern observed for *Glu^{ACh}-GAL4*, indicating that *VGluT* is both transcribed and translated in this subset of *VAChT*-transcribing neurons (Fig. 1I). However, FLP derepression of *ECFP::VAChT* with *VGluT-GAL4* produces no detectable protein in adult brain (Fig. 1I), suggesting either degradation or translational suppression of *VAChT* mRNA in Glu^{ACh} cells. GABA^{ACh} neurons behaved similarly: *EGFP::VGAT* expression confirmed transcription and translation of *VGAT* mRNA, while the absence of ECFP::VAChT protein shows that there is no translation of *VAChT* mRNA in GABA^{ACh} neurons. Thus, *VGluT* and *VGAT* are transcribed and translated in Glu^{ACh} and GABA^{ACh} neurons, respectively, while *VAChT* mRNA is transcribed, but either degraded or untranslated, in both groups.

How does the 3′UTR of *VAChT* mRNA regulate its protein expression? Control of protein synthesis by miRs, small noncoding RNAs, which bind to mRNA to initiate degradation or inhibit translation, is widespread and often centered on the 3′UTR of the message (*16*). In silico evaluation of the *VAChT* 3′UTR (www.targetscan.org/fly_72/) identified multiple high-confidence binding sites for miR-190, an miR that also targets several other cholinergic mRNAs, including *ChAT*, acetylcholine′s synthetic enzyme, as well as *ChT*, the choline transporter. To determine whether miR-190 regulates production of cholinergic effector proteins, we assayed its ability to suppress expression of a Firefly luciferase (Fluc) gene that had either the *VAChT* or *ChAT* 3′UTR. Cotransfection of S2 cells with miR-190 and a *Renilla* luciferase (Rluc) control plasmid induces a significant decrease in the Fluc/Rluc ratio with both *VAChT* and *ChAT* 3′UTRs compared to cotransfection with a scrambled miR. No miR-190–dependent decrease is found when the three putative miR-190 binding sites of the *ChAT* 3′UTR are deleted or there is no 3′UTR (Fig. 2A). These results suggest that miR-190 can suppress the expression of cholinergic proteins by directly binding to their 3′UTRs.

To test the idea that miR-190 is responsible for in vivo repression of cholinergic transmission in Glu^{ACh} and GABA^{ACh} cells, we suppressed miR-190 function in specific neurons using upstream activating sequence (UAS)–driven miR-190 sponge lines. These sponge transgenes consist of arrays of miR binding sites and serve to soak up the cognate miR. They can be used to interrogate the roles of miRs in specific cells and are often weaker than a null allele, which can be deployed against miRs that are required for viability (*17*). To validate the specificity and efficacy of the sponges, and to test for the presence of miR-190 in adult glutamatergic cells, we created UAS-driven Fluc reporter lines that had either the *ChAT* 3′UTR or a mutant *ChAT* 3′UTR that had its miR-190 sites deleted. We used *VGluT-GAL4* to coexpress each reporter with either the miR-190 sponge or a scrambled control sponge. Figure 2B shows that the miR-190 sponge can increase expression of the Fluc-*ChAT* 3′UTR transgene in glutamatergic neurons compared to the control sponge. Fluc levels in animals expressing a transgene in which the miR-190 sites were deleted were high and insensitive to miR-190 sponge expression. These results suggest that miR-190 is present in adult glutamatergic neurons and show that its function can be inhibited in vivo by an miR sponge (Fig. 2B).

To explore the role of miR-190 in regulation of endogenous VAChT translation, we asked whether expression of the miR-190 sponge would result in ECFP::VAChT protein expression from our endogenous gene fusion allele in glutamatergic or GABAergic neurons. For both Glu^{ACh} and GABA^{ACh} cells, the miR-190 sponge produced strong ECFP::VAChT protein signal in the split-GAL4 patterns (Fig. 2, C and D, and fig. S4). These results provide another piece of evidence that *VAChT* is transcribed in Glu^{ACh} and GABA^{ACh} neurons, and they show that miR-190 suppresses accumulation of *VAChT* protein in adult heads. Expression of the miR-190 sponge does not change the expression pattern or intensity of EGFP::VGluT or EGFP::VGAT protein in FSB or EB neurons (Fig. 2, E to H), suggesting that miR-190 has no role in the regulation of VGluT or VGAT protein levels.

The circuitry controlling sleep in *Drosophila* includes regions that contain Glu^{ACh} (dFSB) and GABA^{ACh} (EB) neurons (*18*). Suppression of miR-190 function pan-neuronally, as well as in either glutamatergic (*VGluT-GAL4*) or cholinergic (*ChAT-GAL4*) neurons, reduces daytime and nighttime sleep significantly (fig. S5, A to C) compared to expression of a scrambled control sponge. To ask whether the *ChAT-GAL4* phenotype was the result

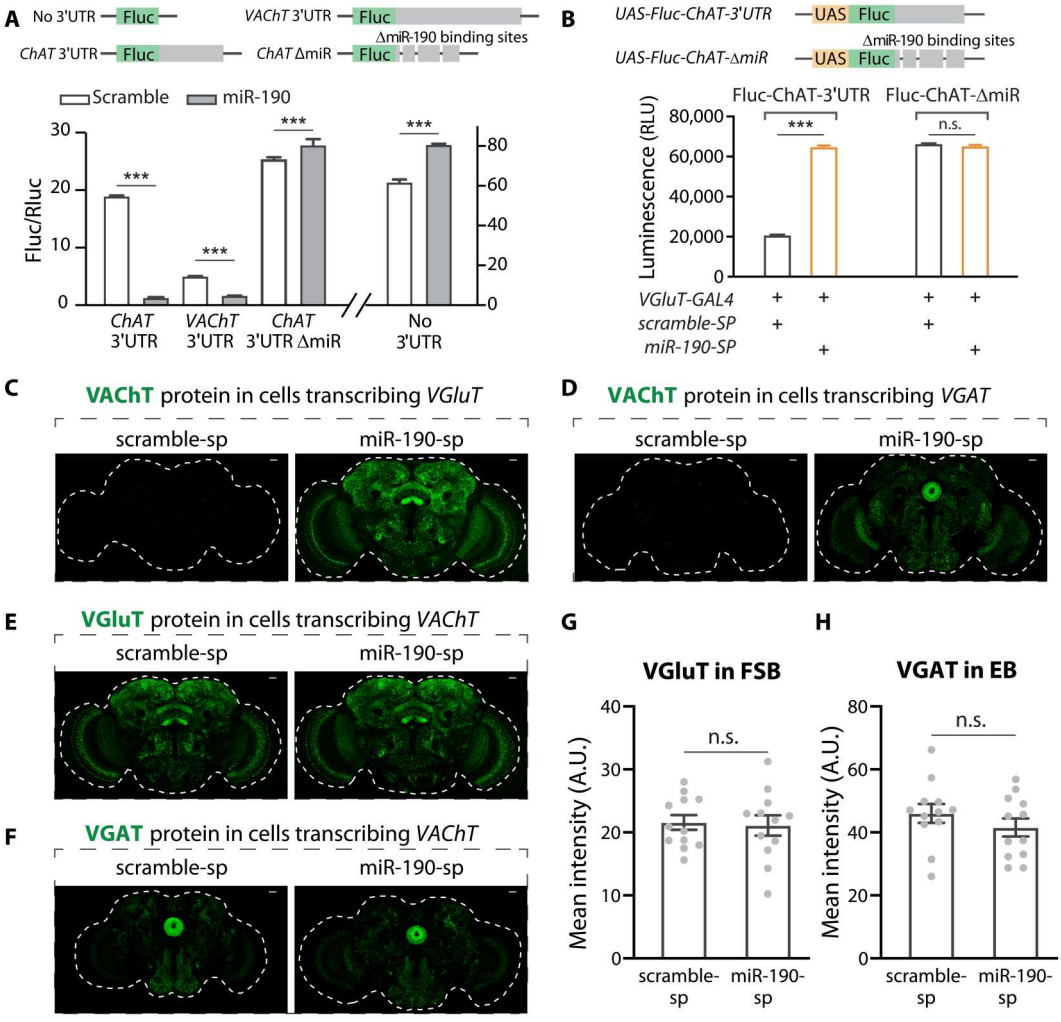

Fig. 2. miR-190 blocks VAChT protein accumulation. (**A**) S2 cells were cotransfected with Fluc-UTR, Rluc, and scramble or miR-190 plasmids. For the no 3′UTR plasmid, only Fluc is included; for the VAChT-3′UTR and ChAT-3′UTR plasmids, Fluc is followed by 3′UTR of *VAChT* or *ChAT*; for the ChAT-del plasmid, the three predicted miR-190 binding sites in the *ChAT* 3′UTR are deleted. Fluc activity was normalized to Rluc activity. $n = 6$ for each group. Coexpression of miR-190 blocks Fluc expression only when plasmids contain *VAChT* or *ChAT* 3′UTRs. Deletion of predicted miR-190 binding sites in the *ChAT* 3′UTR blocks miR-190 suppression. (**B**) Expression of miR-190 sponge in VGluT-positive neurons up-regulates luciferase activity when the Fluc transgene has a *ChAT* 3′UTR, indicating that miR-190 is expressed in these adult neurons. When miR-190 binding sites are deleted from the transgene's *ChAT* 3′UTR, luciferase activity is no longer responsive to miR-190 sponge. $n = 6$ for each group. RLU, relative luminescence unit. (**C** and **D**) Representative pictures of *VGluT-GAL4* (C) or *VGAT-GAL4* (D) driving flip-out derepression of *ECFP::VAChT* flies, with scramble or miR-190 sponge expressed in the same neurons. (**E** and **F**) Representative pictures of *VAChT-GAL4* driving flip-out derepression of *EGFP::VGluT* (E) or *EGFP::VGAT* (F) while expressing scramble or miR-190 sponge in the same neurons. (**G**) Quantification of EGFP::VGluT protein in FSB neurons from (E). (**H**) Quantification of EGFP::VGAT protein in EB neurons from (F). $n = 12$ for each group in (G) and (H). Dashed white lines indicate the whole brain. Scale bars, 20 μm. Data are shown as means ± SEM and analyzed by Student's *t* test. n.s. indicated no difference; $^{***}P < 0.001$. Gray dots show individual values in (G) and (H). A.U., arbitrary units.

of reducing miR-190 function in Glu^{ACh} neurons, we used *VGluT-GAL80* to block GAL4 action in the Glu^{ACh} subpopulation of *ChAT-GAL4*–positive cells. Blocking sponge expression in the Glu^{ACh} class of cholinergic neurons rescued sleep levels and partially rescued the episode duration phenotype (Fig. 3A). Consistent with this, suppression of miR-190 function only in Glu^{ACh} neurons using *Glu^{ACh}-GAL4* split drivers leads to a large reduction in total sleep (Fig. 3B). Together, this demonstrates that loss of miR-190 in Glu^{ACh} cells decreases sleep. Suppression of miR-190 function in GABAergic neurons (fig. S5D) or specifically in GABA^{ACh} cells (Fig. 3C) also decreases nighttime sleep, but to a lesser extent than Glu^{ACh} manipulations. However, miR-190 sponge in either Glu^{ACh} or GABA^{ACh} neurons can generate significant sleep fragmentation (Fig. 3, A to C, and figs. S6 and S7). Locomotor activity while awake is unaffected or reduced by these manipulations (fig. S8), indicating that the decrease of sleep is not due to hyperactivity.

We reasoned that if the sleep effects of miR-190 suppression were due to excess cholinergic transmission in glutamatergic neurons, then expressing both ChAT and VAChT in these neurons should phenocopy the effects of the miR-190 sponge. *Glu^{ACh}-GAL4*–driven expression of ChAT and VAChT transgenes lacking native gene 3′UTR sequences (to ensure protein expression) was completely lethal before adult eclosion, suggesting that the miR-190 suppression of these two proteins in glutamatergic

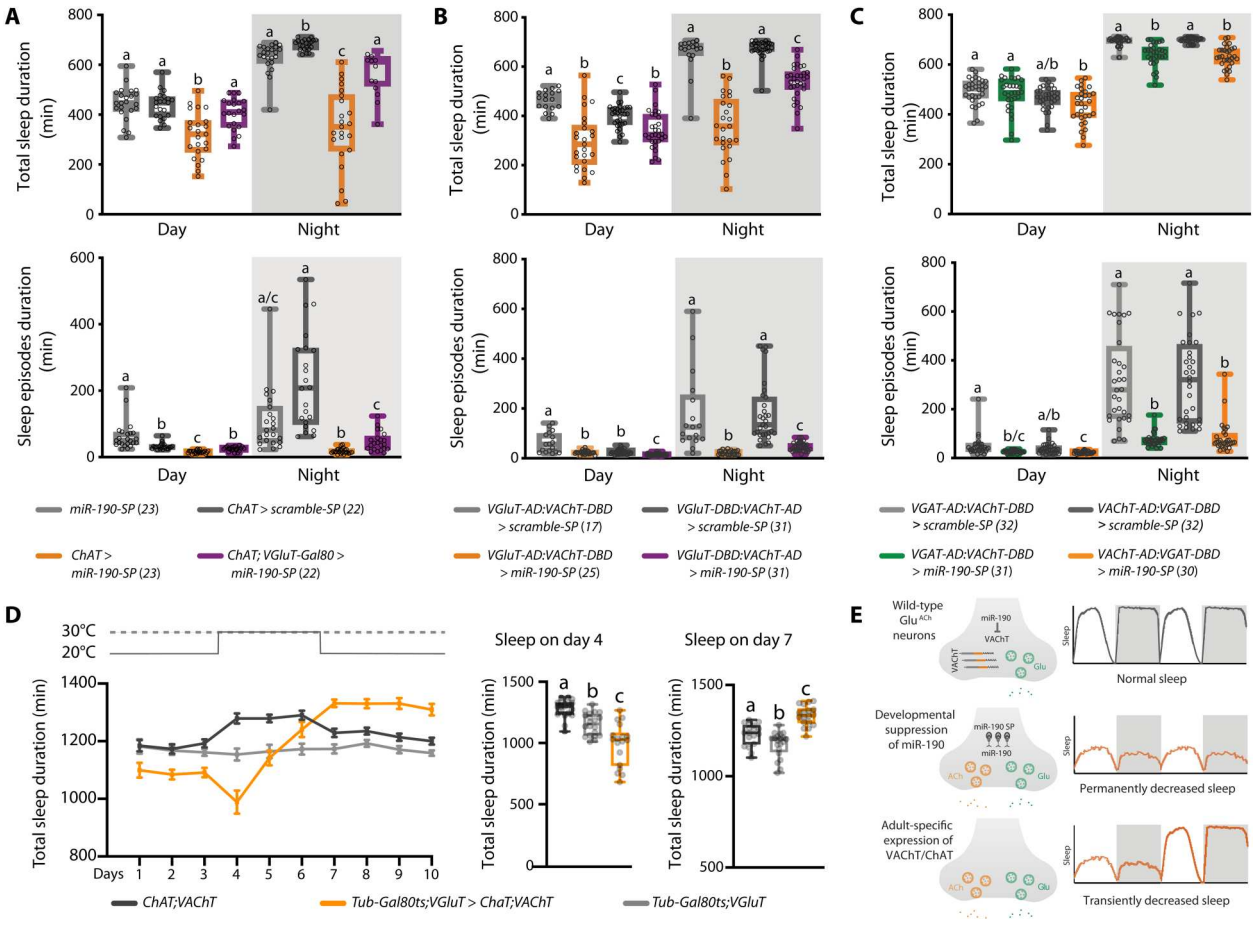

Fig. 3. MiR-190 regulates sleep by controlling cholinergic cotransmission in glutamatergic neurons. (**A**) Reduction and fragmentation of sleep by suppression of miR-190 function in cholinergic neurons maps to neurons also expressing VGluT. (**B**) In *Glu*^{ACh}-GAL4 neurons, miR-190 suppression reduces and fragments daytime and nighttime sleep. (**C**) In *GABA*^{ACh}-GAL4 neurons, miR-190 suppression reduces and fragments daytime and nighttime sleep. (**D**) Temporally controlled overexpression of ChAT and VAChT from transgenes lacking cognate 3′UTRs in VGluT^{+} neurons decreases sleep acutely and triggers fast compensation. n = 18 to 20. Data are shown as means ± SEM; gray circles show individual values. Statistical differences are indicated by letters, with genotypes that are not significantly different having the same letter. (**E**) Summary model and hypothesis. In Glu^{ACh} neurons, suppression of miR-190 function during development induces ACh cotransmission and alters adult sleep circuits. Adult-specific expression of VAChT/ChAT decreases sleep acutely and triggers strong homeostatic compensation.

neurons is required during development. Limiting expression to adulthood with *TubGAL80*^{ts} rescued viability and was sufficient to immediately both decrease and severely fragment sleep (Fig. 3D and fig. S9, A and B). Total sleep recovered rapidly, even before the end of protein induction (Fig. 3D and fig. S9C), perhaps indicative of a strong homeostatic response to the sleep loss induced by expression of cholinergic release machinery. While these data support the idea that cotransmission of ACh is a key part of the adult sleep phenotype, failure to completely recapitulate the miR-190 sponge phenotype implies that there are additional effects on the sleep circuitry when miR-190 function is attenuated using GAL4 drivers whose expression is not limited to the adult (Fig. 3E).

The adult persistence of the miR-190 mechanism for suppression of cholinergic transmission raises the question of whether there are situations where cotransmission is permitted as a form of plasticity. While steady-state VAChT accumulation in normal Glu^{ACh} or GABA^{ACh} cells is not detectable (Fig. 1I), limited local or transient expression would be difficult to visualize. To capture transient events, we designed a "translation-trap" (Fig. 4A). The FLP recombinase coding region was inserted into the *VAChT* locus. FLP-encoding mRNA is translated only under conditions permissive for *VAChT* mRNA translation. Combining this allele with *FRT-stop-FRT-EGFP::VGluT* and *VGAT* alleles should mark Glu^{ACh} and GABA^{ACh} neurons that have translated *VAChT* mRNA at some point in their lifetime. Figure 4B shows EGFP::VGluT staining, indicating that there are Glu^{ACh} neurons in the pars intercerebralis and ventral areas of the brain that have translated *VAChT* mRNA. Similarly, EGFP::VGAT signals in EB, medulla, and several other central brain regions demonstrate translation of *VAChT* in GABA^{ACh} neurons (Fig. 4C). These data show that miR-190 function appears to be transiently suppressed in multiple neuron groups.

Because our translation-trap is an irreversible mark, it does not indicate when or for how long *VAChT* mRNA translation occurred, or whether translation was induced by some physiological cue. To ask whether VAChT translation was occurring in adults, we returned to animals in which VAChT in GABA^{ACh} cells is tagged with enhanced cyan fluorescent protein (ECFP) (Fig. 1H). While

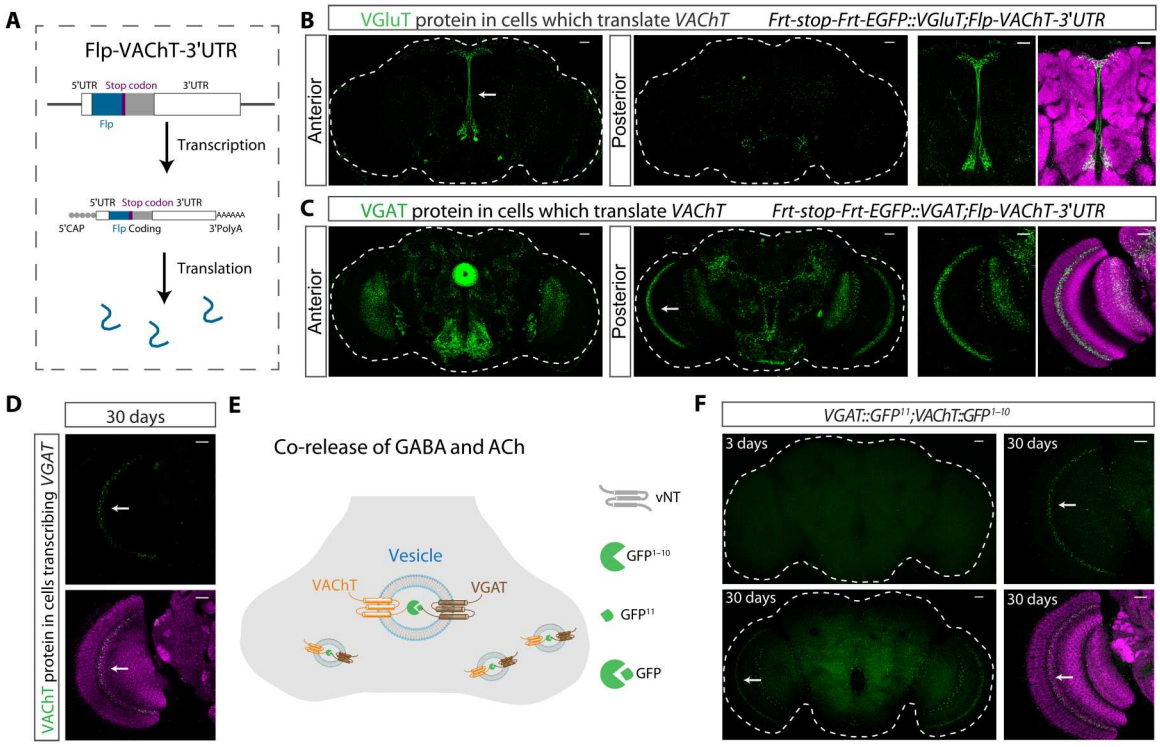

Fig. 4. VAChT repression can be released in specific cell types, and VAChT traffics to VGAT-containing vesicles. (**A**) Schematic diagram showing the translation-trap strategy. In *Flp-VAChT-3′UTR* flies. *Flp* is transcribed and translated as part of the full 3′UTR-containing *VAChT* mRNA. (**B**) *Flp-VAChT-3′UTR* flip-out derepression of *EGFP::V-GluT* marks central brain neurons. The white arrow shows the region enlarged at the right. (**C**) *Flp-VAChT-3′UTR* flip-out derepression of *EGFP::VGAT* medulla and central brain neurons. The white arrow shows the region enlarge at the right. (**D**) In 30-day-old flies, *VGAT-GAL4* flip-out derepression of *ECFP::VAChT* (strategy as in Fig. 1H) generates ECFP signal in medulla (white arrows). (**E**) Schematic of strategy to visualize VAChT localization. *VAChT* and *VGAT* alleles were generated with lumenal split GFP fusions. GFP reconstitution only occurs if VAChT and VGAT are in the same vesicle. (**F**) In 30-day-old flies, reconstituted GFP signal is visible without staining in medulla neurons. In 3-day-old flies, no GFP is detected. For (B) to (D) and (F), green shows EGFP or ECFP, while magenta is Brp staining. Scale bars, 20 μm.

ECFP::VAChT was undetectable in young animals (Fig. 1I), it appears in GABA^{ACh} medulla neurons in 30-day-old brains, consistent with results from the translation-trap showing that these cells can translate VAChT (Fig. 4D). VGAT expression in GABA^{ACh} neurons did not change with age (fig. S10), indicating that these cells may cotransmit ACh and GABA. These data demonstrate that VAChT translation occurs in mature GABA^{ACh} neurons and is associated with aging.

Although the appearance of VAChT protein in nerve terminals is consistent with the packaging of ACh, we sought to determine whether the protein was in synaptic vesicles. We knocked *GFP$^{1–10}$* and *GFP^{11}* into the *VAChT* gene, as well as *GFP^{11}* into the *VGAT* gene (fig. S11, A and B), such that the split GFP would be on the luminal side of the vNT. This orientation allows reconstitution of GFP only when VAChT and VGAT are present in the same vesicle (fig. S11C). Notably, in 30-day-old flies, we found clear reconstitution of live GFP signals between VAChT-GFP$^{1–10}$ and VGAT-GFP^{11} in medulla neurons; no signal was found in 3-day-old animals (Fig. 4, E and F). These results show that VAChT and VGAT are present in the same vesicles and suggest that ACh and GABA can be co-released in aging flies. While functional co-release has yet to be demonstrated, it is notable that aging in flies, such as in humans, is associated with significant increases in sleep fragmentation (*19*), a phenotype of down-regulation of miR-190 function in GABA^{ACh} cells.

DISCUSSION

Cotransmission is now recognized as a common and important mode of neuronal communication, and it can be dynamic. NT plasticity involving replacement of one transmitter with another, either developmentally (*20*) or in the context of a few neurons in a mature circuit (*4*, *21*), has been shown in multiple species. In cases where the molecular mechanism is known, these switching events have ultimately required transcriptional changes (*22*, *23*). In this study, we describe a mechanistically distinct phenomenon in which the transcription of cholinergic genes is already active in thousands of GABAergic and glutamatergic neurons in the adult fly brain, but functional expression is controlled by a reversable miR switch. Because GABA and glutamate are generally inhibitory transmitters in the central brain of *Drosophila*, this gives Glu^{ACh} and GABA^{ACh} neurons the ability to rapidly and transiently alter the magnitude or even the sign of their output by scaling miR-190 levels. These neurons may be akin to the reserve pool neurons of the adult zebrafish spinal cord that can reversibly acquire and release glutamate to enhance neuromuscular junction function acutely after locomotor stress (*24*).

While the extent and the full range of triggers controlling the potential for transmitter plasticity in these cells are unknown, we show that there are certain cell populations that reliably turn on VAChT translation (Fig. 4, B and C), some in response to aging (Fig. 4, D to F). The cell specificity of the translation-trap marks

argues against the signal being due to some sort of "leakiness" and may even indicate that epochs of cholinergic cotransmission may be a normal part of the development or function of these particular neurons. How transient release from miR-190 suppression is accomplished will require further study; however, there are many examples of regulated miR degradation (*25*), one of which has been shown to control miR-190 levels (*26*).

It is also interesting to consider whether posttranscriptional processes may provide a more general mode of fast, but transient, control of transmission. It is notable that *VGAT* mRNA was present in both $GABA^{ACh}$ nuclei and, more unexpectedly, in Glu^{ACh} nuclei (Fig. 1D). The transcription of *VGAT* in Glu^{ACh} neurons, combined with the stochastic EB mCD8::GFP signal seen with *VGAT/VGluT* split-GAL4s (fig. S1, E and F), raises the possibility that there may be non–miR-190–dependent posttranslational regulation of VGAT levels in some glutamatergic neurons. Rapid posttranscriptional modulation of cotransmission provides a powerful mechanism for sculpting behavior in response to external and internal signals.

MATERIALS AND METHODS

Fly strains and husbandry

All flies were raised on standard food at 25°C with a 12-hour light:12-hour dark cycle, except for the *Tubulin-Gal80^{ts}* experiments to induce expression at different developmental stages, where flies were raised at either 18° or 29°C. Male and female flies were collected at eclosion and aged as specified before performing experiments. *VT030559-GAL4* was obtained from the Vienna Drosophila Resource Center stock center. *VAChT$^{[MI08244]}$* (#55439), *nsyb-GAL4* (#51941), *VGluT-GAL4* (#60312), *VGluT-p65-AD* (#82986), *VGluT-GAL4-DBD* (#60313), *ChAT-GAL4* (#60317), *GH146-GAL4* (#30026), *GMR81C04-GAL4* (#48378), *VGAT-GAL4* (#84696), *UAS-miR-190-sponge* (#61397), *UAS-scramble-sponge* (#61501), *UAS-Flp* (#4539), *UAS-CD4-GFP$^{1–10}$* (#93016), *VGluT-Gal80* (#58448), and *tubulin-Gal80^{ts}* (#7016) were obtained from Bloomington *Drosophila* Stock Center. *UAS-myrGFP-2A–RedStinger* (*27*) was obtained from the Ganetzky laboratory at University of Wisconsin, and *UAS-UNC84::GFP* was from G. Henry at Janelia Research Campus. Table S1 lists all the lines used in this study with their source and whether their mRNA contains the native gene's 3′UTR. Table S2 lists the full genotypes of all lines used in this study by figure panel.

Generation of *EGFP::VAChT*, *RFP::VGluT*, and *RFP::VGAT* lines

To knock in *EGFP* at the N terminus of *VAChT*, we designed a guide RNA that recognized the beginning of *VAChT* with an online tool (http://targetfinder.flycrispr.neuro.brown.edu/) and created a donor plasmid (pMC1-EGFP-VAChT plasmid in data S1). The guide RNA was cloned into a pU6 plasmid (Addgene, #45946) and injected into Cas9 flies (*y,sc,v; nos-Cas9/CyO;* +/+) with the donor plasmid. By the same strategy, we knocked in *RFP* at the N terminus of *VGluT* and *VGAT*. All guide RNAs are listed in table S3, and donor plasmids are shown in data S1. Correct integrations were confirmed by polymerase chain reaction (PCR) and sequencing with primers that bind outside the regions of the integrated junction.

Creation of *Frt-stop-Frt-ECFP::VAChT*, *Frt-stop-Frt-EGFP::VGluT*, and *Frt-stop-Frt- EGFP::VGAT* flies

For the *Frt-stop-Frt-ECFP::VAChT* fly strain, we used the same guide RNA as *EGFP::VAChT* and made a donor plasmid (pMC10-Frt-stop-3p3-RFP-Frt-ECFP::VAChT plasmid in data S1). We amplified the stop sequence that was flanked by two Frt sites, *ECFP* sequence, and *VAChT* sequence. 3P3 RFP sequence was amplified and inserted between stop and the second Frt site for screening. These fragments were assembled in order and cloned into the pMC10 plasmid. The guide RNA was cloned into pU6 plasmids and injected into Cas9 flies with the donor plasmid. F_1 progenies with RFP markers were selected as candidates, and further confirmation was performed by PCR and sequencing. By the same strategy, we made *Frt-stop-Frt-EGFP::VGluT* and *Frt-stop-Frt-EGFP::VGAT* flies. The guide RNAs are listed in table S3, and the donor plasmids were shown as pMC10-Frt-stop-3P3-RFP-Frt-EGFP::VGluT and pMC10-Frt-stop-3P3-RFP-Frt-EGFP::VGAT in data S1.

Creation of *Flp-VAChT-3′UTR* flies

For the *Flp-VAChT-3′UTR* fly strain, we used the same guide RNA as *EGFP::VAChT* and made a donor plasmid (pMC10-Flp-VAChT-3′UTR plasmid in data S1). The guide RNA was cloned into the pU6 plasmid and injected into Cas9 flies with the donor plasmid. Correct integrations were confirmed by PCR and sequencing.

Creation of split-GAL4 lines

To make the *VAChT-AD* and *VAChT-DBD* fly strains, the phase 0 T2A-p65AD-Hsp70 plasmid (Addgene, #62914) and T2A-GAL4DBD-Hsp70 plasmid (Addgene, #62903) were injected into *VAChT$^{[MI08244]}$* flies with pBS130 plasmid (Addgene, #26290), which encodes phiC31 integrase. Progenies were crossed to *yw* flies to check for spGAL4 insertion. Male flies with yellow marker were selected as candidates and then checked by PCR to obtain insertion lines in the correct orientation.

For the *VGAT-AD* and *VGAT-DBD* lines, we first made a *3P3-RFP-VGAT* fly strain using the same guide RNA as *RFP::VGAT* (table S3) and a donor plasmid that contained attp flanked *3P3-RFP* sequences (fig. S1A). Flies were first screened for RFP expression and then confirmed by PCR and sequencing. To make *VGAT-AD* flies, the AD sequence was amplified from the T2A-p65AD-Hsp70 plasmid (Addgene, #62914) and attached at the N terminus of the *VGAT* sequence. The whole AD sequence that was flanked by two inverted attB sites was cloned into the pBS-KS-attB2 plasmid (Addgene, #62897). This plasmid was injected into *3P3-RFP-VGAT* flies, with plasmids that expressed phiC31 recombinase. By the same strategy, we made *VGAT-DBD* flies using T2A-GAL4DBD-Hsp70 plasmid (Addgene, #62903). F_1 progenies without RFP marker were selected as candidates, and further confirmation by PCR and sequencing was performed.

Creation of *VAChT-GFP$^{1–10}$*, *VAChT-GFP^{11}*, and *VGAT-GFP^{11}* lines

To make the *VAChT-GFP$^{1–10}$* and *VAChT-GFP^{11}* fly strains, we first chosen a luminal-side insertion site using in silico prediction (https://phobius.sbc.su.se/). We used the same guide RNA as *EGFP::VAChT* and created donor plasmids (VAChT-GFP1-10 plasmid and VAChT-GFP11 plasmid in data S1). The guide RNA was cloned into a pU6 plasmid and injected into Cas9 flies with

the donor plasmids. Correct integrations were confirmed by PCR and sequencing.

For the *VGAT-GFP*^{11} line, a luminal-side insertion site was chosen using in silico prediction (https://phobius.sbc.su.se/). The *GFP*^{11} sequence was inserted at the last luminal side site of the *VGAT* gene. The whole sequence was flanked by two inverted attB sites and cloned into the pBS-KS-attB2 plasmid (Addgene, #62897). This plasmid (VGAT-GFP11 plasmid in data S1) was injected into *3P3-RFP-VGAT* flies showed above, with plasmids that expressed phiC31 recombinase. F_1 progenies without RFP marker were selected as candidates, and further confirmation by PCR and sequencing was performed. Luminal location of the tags was confirmed as shown in fig. S11.

Creation of *UAS-ChAT*, *UAS-VAChT*, *UAS-Fluc-ChAT 3′UTR*, and *UAS-Fluc-ChAT del* lines

For the *UAS-RFP::ChAT* fly strain, the coding region of *ChAT* was amplified from a *Canton-S* wild-type fly cDNA library and inserted into the pUAST-attB plasmid (8489 base pairs; Addgene) using the Gibson assembly method (UAS-RFP::ChAT plasmid in data S1). To allow visualization of ChAT expression, RFP was inserted in frame before the ChAT coding region. Using the same strategy, *GFP1–10* and *VAChT* coding regions were amplified and inserted into pUAST-attB to make the *UAS-VAChT* fly line (UAS-GFP1-10::VAChT plasmid in data S1).

For the *UAS-Fluc-ChAT 3′UTR* fly line, we amplified the Fluc sequence from the Ac/Fluc plasmid (a gift of R. Allada) and the ChAT 3′UTR sequence from the *Canton-S* wild-type fly genome. These sequences were assembled in order and cloned into the pUAST-attB plasmid (UAS-Fluc-ChAT 3′UTR plasmid in data S1). For the *UAS-Fluc-ChAT del* fly line, the same sequences were used, except that the predicted miR-190 binding sites were removed from ChAT 3′UTR (UAS-Fluc-ChAT del plasmid in data S1).

All plasmids were checked by sequencing. UAS-RFP::ChAT, UAS-Fluc-ChAT 3′UTR, and UAS-Fluc-ChAT del plasmids were injected into *phiC31-attP* flies (Bloomington *Drosophila* Stock Center, #79604), which have an attP site on the second chromosome to allow targeted integration. UAS-GFP1–10::VAChT plasmid was injected into *phiC31-attP* flies (Bloomington Stock Center, #8622), which have an attP site on the third chromosome. The progeny of injected flies was screened for w^+ red eye marker and then checked by PCR and sequencing.

INTACT purification of nuclei

Nuclei from *Glu*^{ACh} > *UNC84::GFP* and *GABA*^{ACh} > *UNC84::GFP* heads were prepared according to the INTACT protocol (*13*), with some adjustments. Briefly, whole flies were flash-frozen on dry ice in 15-ml tubes and vortexed for 5 cycles of 15-s vortexing at max speed and 1 min of resting on dry ice. Heads were separated from bodies using frozen no. 40 and no. 25 brass sieves. Sieved heads were placed in prechilled 1-ml Dounce homogenizers and homogenized using a modified INTACT lysis buffer [10 mM tris-HCl (pH 7.5), 2 mM $MgCl_2$, 10 mM KCl, 0.6 mM spermidine, 0.2 mM spermine, 1 mM dithiothreitol, 0.03% Tween 20, 1% bovine serum albumin, and 1× cOmplete protease inhibitor] for 15 strokes with pestle A and 15 strokes with pestle B. The homogenized lysate was filtered through a 20-μm CellTrics filter (Sysmex Flow Cytometry), centrifuged for 5 min at 800 relative centrifugal force (RCF). The supernatant was removed and the lysate was resuspended in modified INTACT lysis buffer and filtered through a 10-μm CellTrics filter (Sysmex Flow Cytometry). The filtered lysate was then subject to anti-GFP immunoprecipitation and RNA extraction as previously described (*13*).

RNA-seq and data analysis

Purified RNA was subject to polyA enrichment using the Poly(A)-Purist Mag Kit (Thermo Fisher Scientific) according to the protocol. Purified polyA RNA was quantified using the Qubit 2.0 RNA HS assay (Thermo Fisher Scientific), and 10 ng of RNA per sample was used for library prep using the NextFlex Rapid Directional qRNA-Seq Kit 2.0 (PerkinElmer) and sequenced on a NextSeq 550 using the 75-cycle High Output Kit (Illumina).

Unique molecular identifiers (UMIs) were extracted and appended to reads from sequenced libraries using umI_tools extract with the following parameters: --bc-pattern=NNNNNNNNN --bc-pattern2=NNNNNNNNN. Processed reads were then aligned against the dm6 reference genome with STAR using the following parameters: --outFilterMismatchNoverLmax 0.05 --outFilterMatchNmin 15 –outFilterMultimap Nmax 1 --outSJfilterReads Unique --alignMatesGapMax 25000. Aligned reads were converted to BAM files, sorted using samtools, and deduplicated using umi_tools dedup. Reads were counted using featurecounts, and normalization and differential expression was conducted using Deseq2. The full dataset is available at the National Center for Biotechnology Information, Gene Expression Omnibus accession number GSE221859.

Immunohistochemistry and image processing

For dissection and staining of adult fly brains, the protocol from Janelia (www.janelia.org/project-team/flylight/protocols) was used. Briefly, brains were dissected in S2 solution and then fixed in 2% paraformaldehyde (PFA) solution for 55 min at room temperature (RT). Then, the samples were washed 4 × 10 min by 0.5% phosphate-buffered saline with Triton X-100 (PBST) solution and blocked with 5% goat serum in PBST solution for 1.5 hours. After that, the samples were incubated in primary antibody solution for 4 hours at RT and continued incubation at 4°C for over two nights. Then, samples were washed 3 × 30 min by 0.5% PBST and incubated in secondary antibody solution for 4 hours at RT, with continued incubation at 4°C for over three nights. The same washing protocol was performed after secondary antibody incubation, then fixed by 4% PFA again for 4 hours at RT, and mounted in VECTASHIELD mounting medium (Vector Laboratories).

The primary antibodies used were rabbit anti-RFP (1:200; Takara), rabbit anti-GFP (1:1000; Thermo Fisher Scientific), mouse anti-GFP (1:200; Sigma-Aldrich), mouse anti-Brp (1:100; DSHB), anti-VGluT (1:200; gift from A. DiAntonio, Washington University) (*28*), and anti-VGAT (1:200; gift from D. Krantz, University of California Los Angeles) (*29*). Alexa Fluor 488 anti-mouse/rabbit antibody (Invitrogen) and Alexa Fluor 635 anti-mouse/rabbit antibody (Invitrogen) were used as secondary antibodies at 1:200 dilutions.

All images were taken using a Leica SP5 confocal microscope under ×20 or ×60 objective lens. Then, the pictures are processed and analyzed using ImageJ Fiji software (*30*).

Sleep and locomotor activity

Individual 3- to 5-day-old male flies were loaded into 65-mm by 5-mm glass tubes (Trikinetics, Waltham, MA) using CO_2 anesthesia. One end of the tube is food containing 5% agarose and 2% sucrose, and the other side is a cotton ball to cover it. The flies were entrained under standard 12-hour light:12-hour dark conditions for 2 days before data collection.

Locomotor activity was collected with the *Drosophila* Activity Monitoring System (Trikinetics) as previously described (*31*). Sleep is defined as consecutive inactivity for five or more minutes (*32*). All sleep parameters, including total sleep duration, number of sleep episodes, and mean episode duration were analyzed using a Matlab program described previously (*31*) and averaged across 4 days. Statistical analysis was performed with GraphPad Prism. For all sleep parameters, a D′Agostino and Pearson test was used to determine normality of data. If data were normally distributed, then they were analyzed using a Student's *t* test or analysis of variance (ANOVA) followed by Tukey test for multiple comparisons (depending on the number of groups). If data were not normally distributed, then they were analyzed using a Mann-Whitney or Kruskal-Wallis test followed by Dunn's test for multiple comparisons.

S2 cell assay

S2 cells (*33*) in 12-well plates were cotransfected with 15 ng of Ac/Fluc (or its derivatives), 15 ng of Ac/Rluc, and 270 ng of Ac/miR-190 or Ac/scramble using an Effectene transfection reagent (QIAGEN). Ac/Fluc derivatives included Fluc with *ChAT*-3′UTR, Fluc with *VAChT*-3′UTR, and Fluc with *ChAT*-3′UTR with the three predicted miR-190 binding sites removed. The primers are listed in table S4. Cells were harvested 48 hours after transfection, and a dual luciferase assay was performed (Promega).

In vivo luciferase assays

Fifteen male fly brains were collected for each sample and then homogenized in 100 μl of Promega Glo Lysis Buffer (Promega, catalog no. E2510) at RT. Homogenized samples were incubated for 10 min at RT and then centrifuged for 5 min to pellet the brain remains. Fifty microliters of supernatant was transferred to an Eppendorf tube on ice, and another 450-μl lysis buffer was added. A multichannel pipette was used to transfer 20 μl of each sample to a white-walled 96-well plate (Costar), and then 20 μl of Promega Luciferase Reagent (Promega, catalog no. E2510) was added to each well. The plate was incubated in the dark for 10 min. Luminescence was measured on a luminometer plate reader (Promega, catalog no. GM3000).

Supplementary Materials

This PDF file includes:

Supplementary Materials and Methods
Figs. S1 to S11
Tables S1 to S4
Legend for data S1

Other Supplementary Material for this manuscript includes the following:

Data S1

REFERENCES AND NOTES

1. N. Ayala-Lopez, S. W. Watts, Physiology and pharmacology of neurotransmitter transporters. *Compr. Physiol.* **11**, 2279–2295 (2021).
2. K. Silm, J. Yang, P. F. Marcott, C. S. Asensio, J. Eriksen, D. A. Guthrie, A. H. Newman, C. P. Ford, R. H. Edwards, Synaptic vesicle recycling pathway determines neurotransmitter content and release properties. *Neuron* **102**, 786–800.e5 (2019).
3. L. M. Sherer, E. Catudio Garrett, H. R. Morgan, E. D. Brewer, L. A. Sirrs, H. K. Shearin, J. L. Williams, B. D. McCabe, R. S. Stowers, S. J. Certel, Octopamine neuron dependent aggression requires dVGLUT from dual-transmitting neurons. *PLOS Genet.* **16**, e1008609 (2020).
4. N. C. Spitzer, Neurotransmitter switching in the developing and adult brain. *Annu. Rev. Neurosci.* **40**, 1–19 (2017).
5. A. J. Granger, M. L. Wallace, B. L. Sabatini, Multi-transmitter neurons in the mammalian central nervous system. *Curr. Opin. Neurobiol.* **45**, 85–91 (2017).
6. S. Kim, M. L. Wallace, M. El-Rifai, A. R. Knudsen, B. L. Sabatini, Co-packaging of opposing neurotransmitters in individual synaptic vesicles in the central nervous system. *Neuron* **110**, 1371–1384.e7 (2022).
7. K. Pankova, A. Borst, RNA-Seq transcriptome analysis of direction-selective T4/T5 neurons in Drosophila. *PLOS ONE* **11**, e0163986 (2016).
8. V. Croset, C. D. Treiber, S. Waddell, Cellular diversity in the Drosophila midbrain revealed by single-cell transcriptomics. *eLife* **7**, e34550 (2018).
9. H. Lacin, H. M. Chen, X. Long, R. H. Singer, T. Lee, J. W. Truman, Neurotransmitter identity is acquired in a lineage-restricted manner in the Drosophila CNS. *eLife* **8**, e43701 (2019).
10. M. P. Nusbaum, D. M. Blitz, E. Marder, Functional consequences of neuropeptide and small-molecule co-transmission. *Nat. Rev. Neurosci.* **18**, 389–403 (2017).
11. A. J. Granger, N. Mulder, A. Saunders, B. L. Sabatini, Cotransmission of acetylcholine and GABA. *Neuropharmacology* **100**, 40–46 (2016).
12. H. Luan, N. C. Peabody, C. R. Vinson, B. H. White, Refined spatial manipulation of neuronal function by combinatorial restriction of transgene expression. *Neuron* **52**, 425–436 (2006).
13. J. Ma, V. M. Weake, Affinity-based isolation of tagged nuclei from Drosophila tissues for gene expression analysis. *J. Vis. Exp.*, 51418 (2014).
14. B. W. Solnestam, H. Stranneheim, J. Hallman, M. Kaller, E. Lundberg, J. Lundeberg, P. Akan, Comparison of total and cytoplasmic mRNA reveals global regulation by nuclear retention and miRNAs. *BMC Genomics* **13**, 574 (2012).
15. C. Mayr, Regulation by 3′-untranslated regions. *Annu. Rev. Genet.* **51**, 171–194 (2017).
16. S. Jonas, E. Izaurralde, Towards a molecular understanding of microRNA-mediated gene silencing. *Nat. Rev. Genet.* **16**, 421–433 (2015).
17. T. A. Fulga, E. M. McNeill, R. Binari, J. Yelick, A. Blanche, M. Booker, B. R. Steinkraus, M. Schnall-Levin, Y. Zhao, T. DeLuca, F. Bejarano, Z. Han, E. C. Lai, D. P. Wall, N. Perrimon, D. Van Vactor, A transgenic resource for conditional competitive inhibition of conserved Drosophila microRNAs. *Nat. Commun.* **6**, 7279 (2015).
18. G. Artiushin, A. Sehgal, The Drosophila circuitry of sleep-wake regulation. *Curr. Opin. Neurobiol.* **44**, 243–250 (2017).
19. K. Koh, J. M. Evans, J. C. Hendricks, A. Sehgal, A Drosophila model for age-associated changes in sleep:wake cycles. *Proc. Natl. Acad. Sci. U.S.A.* **103**, 13843–13847 (2006).
20. E. J. Furshpan, P. R. MacLeish, P. H. O'Lague, D. D. Potter, Chemical transmission between rat sympathetic neurons and cardiac myocytes developing in microcultures: Evidence for cholinergic, adrenergic, and dual-function neurons. *Proc. Natl. Acad. Sci. U.S.A.* **73**, 4225–4229 (1976).
21. D. Dulcis, P. Jamshidi, S. Leutgeb, N. C. Spitzer, Neurotransmitter switching in the adult brain regulates behavior. *Science* **340**, 449–453 (2013).
22. D. Dulcis, G. Lippi, C. J. Stark, L. H. Do, D. K. Berg, N. C. Spitzer, Neurotransmitter switching regulated by miRNAs controls changes in social preference. *Neuron* **95**, 1319–1333.e5 (2017).
23. D. Dulcis, N. C. Spitzer, Reserve pool neuron transmitter respecification: Novel neuroplasticity. *Dev. Neurobiol.* **72**, 465–474 (2012).
24. M. Bertuzzi, W. Chang, K. Ampatzis, Adult spinal motoneurons change their neurotransmitter phenotype to control locomotion. *Proc. Natl. Acad. Sci. U.S.A.* **115**, E9926–E9933 (2018).
25. X. Fu, A. Shah, J. M. Baraban, Rapid reversal of translational silencing: Emerging role of microRNA degradation pathways in neuronal plasticity. *Neurobiol. Learn. Mem.* **133**, 225–232 (2016).
26. C. Y. Shi, E. R. Kingston, B. Kleaveland, D. H. Lin, M. W. Stubna, D. P. Bartel, The ZSWIM8 ubiquitin ligase mediates target-directed microRNA degradation. *Science* **370**, eabc9359 (2020).
27. R. W. Daniels, A. J. Rossano, G. T. Macleod, B. Ganetzky, Expression of multiple transgenes from a single construct using viral 2A peptides in Drosophila. *PLOS ONE* **9**, e100637 (2014).

28. R. W. Daniels, C. A. Collins, K. Chen, M. V. Gelfand, D. E. Featherstone, A. DiAntonio, A single vesicular glutamate transporter is sufficient to fill a synaptic vesicle. *Neuron* **49**, 11–16 (2006).
29. H. Fei, D. M. Chow, A. Chen, R. Romero-Calderon, W. S. Ong, L. C. Ackerson, N. T. Maidment, J. H. Simpson, M. A. Frye, D. E. Krantz, Mutation of the Drosophila vesicular GABA transporter disrupts visual figure detection. *J. Exp. Biol.* **213**, 1717–1730 (2010).
30. J. Schindelin, I. Arganda-Carreras, E. Frise, V. Kaynig, M. Longair, T. Pietzsch, S. Preibisch, C. Rueden, S. Saalfeld, B. Schmid, J. Y. Tinevez, D. J. White, V. Hartenstein, K. Eliceiri, P. Tomancak, A. Cardona, Fiji: An open-source platform for biological-image analysis. *Nat. Methods* **9**, 676–682 (2012).
31. N. C. Donelson, E. Z. Kim, J. B. Slawson, C. G. Vecsey, R. Huber, L. C. Griffith, High-resolution positional tracking for long-term analysis of Drosophila sleep and locomotion using the "tracker" program. *PLOS ONE* **7**, e37250 (2012).
32. J. C. Hendricks, S. M. Finn, K. A. Panckeri, J. Chavkin, J. A. Williams, A. Sehgal, A. I. Pack, Rest in Drosophila is a sleep-like state. *Neuron* **25**, 129–138 (2000).
33. C. Lim, J. Lee, C. Choi, V. L. Kilman, J. Kim, S. M. Park, S. K. Jang, R. Allada, J. Choe, The novel gene *twenty-four* defines a critical translational step in the *Drosophila* clock. *Nature* **470**, 399–403 (2011).

Acknowledgments: We thank E. Dougherty in the Brandeis Imaging Facility for assistance. We also thank P. Garrity, P. Sengupta, and S. Kadener for critical comments on this manuscript. **Funding:** This work was supported by NIH R01067284, NIH R21NS096414, NIH R01067284, and NIH P01NS090994 to L.C.G. M.H. and E.J.R.-R. were supported by NIH T32NS019929, and E.J.R.-R. was supported by NIH F31NS110273. Stocks obtained from the Bloomington Drosophila Stock Center (NIH P40OD018537) were used in this study. **Author contributions:** Conceptualization: L.C.G., Y.Z., N.C., and E.J.R.-R. Methodology: Y.Z., N.C., E.J.R.-R., M.H., and A.D.Y. Investigation: Y.Z., N.C., E.J.R.-R., and A.D.Y. Visualization: Y.Z., N.C., E.J.R.-R., and A.D.Y. Funding acquisition: L.C.G. Supervision: L.C.G. Writing—original draft: N.C. and L.C.G. Writing—review and editing: N.C., Y.Z., M.R., and L.C.G. **Competing interests:** The authors declare that they have no competing interests. **Data and materials availability:** All data needed to evaluate the conclusions in the paper are present in the paper and/or the Supplementary Materials.

Submitted 2 February 2023
Accepted 1 May 2023
Published 2 June 2023
10.1126/sciadv.adg9836